

Chapter 4 - 3D NUMERICAL HYDRO-DYNAMIC MODEL

Chapter 4

3D NUMERICAL HYDRODYNAMIC MODEL

4.1 Introduction

For practical purposes, several types of model representations are used. Fox (1985) has summarized different types of models used in the coastal studies. Of the wide range of models employed in the study of natural systems, numerical models are more successful because of their generality, versatility and flexibility. Numerical models can solve both the linear and nonlinear problems. To solve the equations of the model, numerical methods involving computational procedures have to be used. Model simulation can be considered as a mathematical, logical representation of a system, and then conducting experiments with the computerized system model on a digital computer. Modeling is, therefore, the integrated development of mathematical equations, logical rules and constraints and a computer program embodying the equations, the logical rules and the solutions to them. Simulation on the other hand, is the experimental manipulation of the model on a digital computer. A simulation model has several advantages like:

1. It permits controlled experimentation. A simulation model can be run a number of times with varying input parameters to test the behavior of the system under a variety of situations and conditions.
2. It permits time compression. Operation of the system over extended periods of time can be simulated in only minutes with ultra fast computers.
3. It permits sensitivity analysis by manipulation of input variables.
4. It does not disturb the real natural system.
5. It permits manipulation in terms of real-time of minutes that would take years for the prototype.

4.2 “COSMOS” the 3D Numerical model

COSMOS is a three dimensional hydrodynamic numerical model, initially used by Nakata et al. (1983a) and demonstrated its usefulness successfully in low tide dominated, enclosed coastal bays and inland seas of Japan such as Tokyo bay, Osaka bay, Chinhae bay, etc (Horiguchi, et al., 1998a,b), Oniami bay and lakes of Shinji and Nakaumi (Nakata et al. 1983, 2000), and Ise-Mikawa bay (Taguchi et al., 1999). Five components of tides, wind stress and river run-off, sea surface temperature, chlorinity etc were applied in the model to carry out bay ecosystem studies. Whereas, in present study, COSMOS model is used for the high tide dominated Gulf of Kachchh region to study tidal variation, ocean currents, residual currents and sea surface temperature distribution to understand sediment dispersion and distribution in the Gulf. The environment within the Gulf, in general, varies over a wide range both temporally and spatially because it is affected by dynamic forcing variables such as tide, river discharge, pollutant input, surface winds, and other meteorological parameters; its coastline geometry and bottom topography are usually complicated. And due to this reason, this 3D time-dependent hydrodynamic model is considered for this study.

4.3 Model description

The numerical algorithm of the hydrodynamic model is well described by Nakata et al. (1983a). The model includes time-dependant tidal forcing, surface wind and local density gradients together with actual coastline and bathymetry. Under hydrostatic and Boussinesq approximation on a rotating Cartesian coordinate system, the model employs the equation of fluid motion, flow continuity, conservation of heat and salt to determine the local distribution of prognostic variables i.e. mean velocity components, surface displacement, temperature and salinity. For the equation of state, Knudsen's expression is adopted. In this model, water column is divided into five layers and in each layer

the distribution of current velocity and direction, pressure water temperature, salinity and turbulent energy are computed.

4.4 Basic governing equations

The above fundamental equations are summarized as follows,

1. Momentum equation in x-direction :

$$\frac{\partial u}{\partial t} = -\frac{\partial}{\partial x}(u^2) - \frac{\partial}{\partial y}(uv) - \frac{\partial}{\partial z}(uw) + f_0 v - g \frac{\partial \zeta}{\partial x} - \frac{g}{\rho} \int_z^0 \frac{\partial \rho}{\partial x} dz' - \frac{1}{\rho} \frac{P_a}{\partial x} + \frac{\partial}{\partial x} \left(N_x \frac{\partial u}{\partial x} \right) + \frac{\partial}{\partial y} \left(N_y \frac{\partial u}{\partial y} \right) + \frac{\partial}{\partial z} \left(N_z \frac{\partial u}{\partial z} \right) \quad (4.1)$$

2. Momentum equation in y-direction :

$$\frac{\partial v}{\partial t} = -\frac{\partial}{\partial x}(uv) - \frac{\partial}{\partial y}(v^2) - \frac{\partial}{\partial z}(vw) - f_0 u - g \frac{\partial \zeta}{\partial y} - \frac{g}{\rho} \int_z^0 \frac{\partial \rho}{\partial y} dz' - \frac{1}{\rho} \frac{P_a}{\partial y} + \frac{\partial}{\partial x} \left(N_x \frac{\partial v}{\partial x} \right) + \frac{\partial}{\partial y} \left(N_y \frac{\partial v}{\partial y} \right) + \frac{\partial}{\partial z} \left(N_z \frac{\partial v}{\partial z} \right) \quad (4.2)$$

3. Equation of continuity :

$$\frac{\partial u}{\partial x} + \frac{\partial v}{\partial y} + \frac{\partial w}{\partial z} = 0 \quad (4.3)$$

4. Sea surface (tide) level equation:

$$\frac{\partial \zeta}{\partial t} = -\frac{\partial}{\partial x} \left(\int_{-H}^{\zeta} u dz \right) - \frac{\partial}{\partial y} \left(\int_{-H}^{\zeta} v dz \right) \quad (4.4)$$

5. Temperature distribution equation :

$$\frac{\partial T}{\partial t} = -\frac{\partial}{\partial x}(uT) - \frac{\partial}{\partial y}(vT) - \frac{\partial}{\partial z}(wT) + \frac{\partial}{\partial x} \left(k_x \frac{\partial T}{\partial x} \right) + \frac{\partial}{\partial y} \left(k_y \frac{\partial T}{\partial y} \right) + \frac{\partial}{\partial z} \left(k_z \frac{\partial T}{\partial z} \right) \quad (4.5)$$

6. Chlorinity distribution equation :

$$\frac{\partial Cl}{\partial t} = -\frac{\partial}{\partial x}(u \cdot Cl) - \frac{\partial}{\partial y}(v \cdot Cl) - \frac{\partial}{\partial z}(w \cdot Cl) + \frac{\partial}{\partial x}\left(k_x \frac{\partial Cl}{\partial x}\right) + \frac{\partial}{\partial y}\left(k_y \frac{\partial Cl}{\partial y}\right) + \frac{\partial}{\partial z}\left(k_z \frac{\partial Cl}{\partial z}\right) \text{-----(4.6)}$$

7. State (Knudsen) equation :

$$\rho = \rho(Cl, T)$$

$$\rho = \frac{\sigma_t}{1000} + 1$$

$$\sigma_t = \sum + (\sigma_o + 0.1324)\{1 - A_t + B_t(\sigma_o + 0.1324)\} \text{----- (4.7)}$$

$$\sigma_o = -0.069 + 1.4708CL - 0.001570CL^2 + 0.0000398CL^3 \text{----- (4.8)}$$

$$\sum_t = -\frac{(T - 3.98)^2 \left[\frac{T + 283.0}{T + 67.26} \right]}$$

$$A_t = T(4.7869 - 0.098185T + 0.0010843T^2) \times 10^{-3} \text{----- (4.9)}$$

$$B_t = T(18.030 - 0.8164T + 0.01667T^2) \times 10^{-6} \text{----- (4.10)}$$

Where,

u, v : Advection in x, y directions,

w : Vertical velocity with positive upward.

ζ : Tide surface level,

ρ : Density of sea water,

f_a : Coriolis parameter,

g : Acceleration due to gravity,

T : Temperature,

Cl : Salinity,

N_x, N_y, N_z : Water viscosity in x, y, z directions

k_x, k_y, k_z : Temperature or chlorinity diffusion in x, y, z direction

4.5 Boundary conditions and specifications of the model

Five boundaries are considered in this model like, land-ocean (coastal, island) boundary, air-sea (surface) boundary, sea bottom friction boundary, discharge from river boundary and Gulf-open ocean (open) boundary. Thus the boundary conditions used in COSMOS model include sea surface, sea bottom friction, open boundary and the discharge from rivers along the Gulf of Kachchh.

1. For the sea surface boundary, the average wind stress is calculated using equation (4.11,12),

$$\rho_0 \left(A_z \frac{\partial U}{\partial z}, A_z \frac{\partial V}{\partial z} \right) = (\tau_x, \tau_y) \text{----- (4.11)}$$

$$(\tau_x, \tau_y) = \rho_a C_d (W_x W, W_y W) \text{----- (4.12)}$$

Here ρ_0 is air density (1.2E-3 g/cm³),

Cd drag coefficients,

w_{xy} wind velocity in x, y directions.

2. The sea bottom friction (z=-H) conditions are defined as follows,

$$\rho \left(A_z \frac{\partial U}{\partial z}, A_z \frac{\partial V}{\partial z} \right) = (\tau_x^b, \tau_y^b) \text{----- (4.13)}$$

$$(\tau_x^b, \tau_y^b) = \rho C_b (UW, VW) \text{----- (4.14)}$$

where ρ Sea water density (1.024g/cm³),

(τ_x^b, τ_y^b) Friction stress in the sea bottom,

Cb Friction coefficient of sea bottom.

No slip condition was used at the land boundary.

3. Open Boundary conditions:

A straight boundary line, separating gulf from open sea along the mouth of Gulf, is considered as an Open Boundary for the present model. Following four parameters are considered for initial boundary values while running model :

- Sea Surface Temperature

- Tide components
- Chlorinity (Salinity)
- Sea Surface level

Sea surface temperature (SST) & Chlorinity (Salinity):

Under the ideal conditions, model requires mean monthly SST and salinity profiles within each grid along open boundary. However, due to limited availability of actual field data, SST and salinity are extracted from the available SST and salinity profile (Figure 4.1) measured during November 1997 and is used in all grids along open boundary.

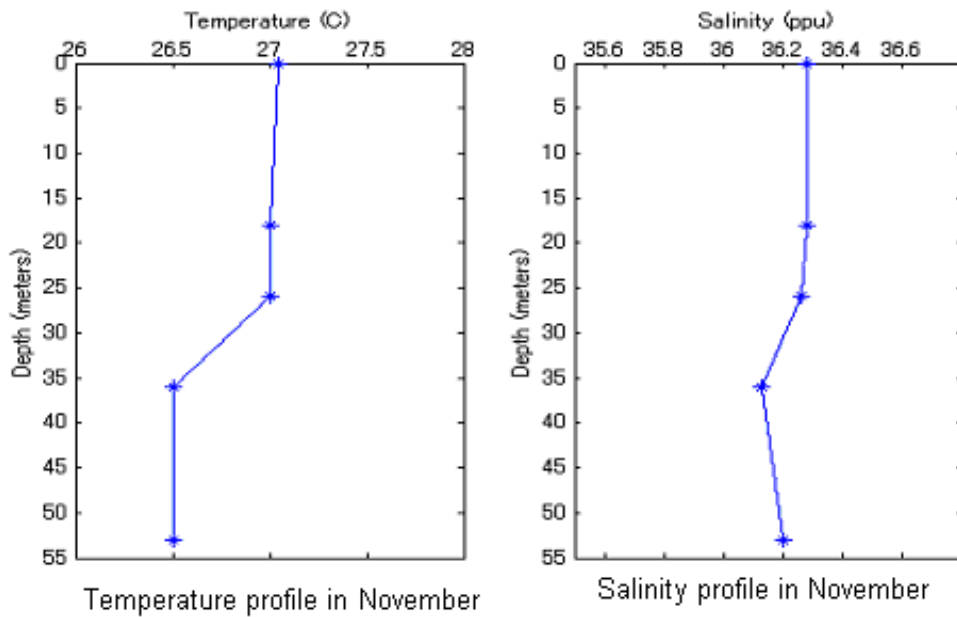


Figure 4.1 Profiles of temperature and salinity measured at the estuary of the Gulf of Kachchh

Tidal components:

COSMOS model ideally requires amplitude and phase values of tide in each grid along open boundary line. There are regular tide measurements at Okha, Kandla and Navlakhi stations. There have been tidal observations at various locations in the Gulf during different epochs. The International

Hydrographic Bureau, Monaco, documents the amplitude and Greenwich phases of various constituents at these stations. Table 4.1 shows the information of important tidal constituents at Port Okha, which is used for constructing the prescribed open boundary conditions for tide.

Consti tuents	Amplitude (cm)	Phase (degree)	Amplitude (cm)	Phase (degree)	Amplitude (cm)	Phase (degree)
M ₂	113.3	208.8	231.6	265.6	247.5	265.5
S ₂	33.5	235.8	75.2	305.0	67.6	304.3
N ₂	25.0	184.4	45.07	253.6	49.4	255.6
K ₁	42.7	235.8	49.4	4.3	51.4	15.1
O ₁	19.8	347.9	23.8	355.3	24.1	7.1

Table 4.1 Important tidal constituents at Port Okha.

Most of the observations are at different epochs and there are no simultaneous observations for simulating tides and hence using the above available data, a composite tide is constructed in the form as follows (Unnikrishnan et al., 1999, Nakano, 1936),

$$\xi(t) = z_0 + \sum A_i f_i \cos\{\sigma_i t - g_i + (V_i + u_i)\} \text{ ----- (4.15)}$$

Where, Z_0 is the mean sea level,

A_i and g_i are amplitude and Greenwich phase of the constituent i respectively,

f_i is node factor,

$(V_i + u_i)$ is astronomical argument,

σ_i is tide frequency.

For the prediction of composite tide, amplitudes and Greenwich phases of the four major constituents at Okha stations in Gulf of Kachchh are considered

and the astronomical arguments are calculated theoretically. In this study, the data are excerpted from Nakano (1936). At the open boundary, the mean sea level at the Gulf is set to 0.01m, which is used for tide forcing. The sea surface elevation was approximated by a sinusoidal oscillation consisting of five dominant constituents in the Gulf. Those were two semi-diurnal constituents, M_2 and S_2 , two diurnal constituents, K_1 and O_1 , and the residual annual constituent, N_2 and the harmonic coefficients and the phase as shown in equation (4.15) are calculated and summarized in Table 4.2.

Tide components	Period (hours)	Amplitude $A_i f_i$ (cm)	Phase(degree) $-g_i + (V_i + u_i)$
M2	12.4	116.4	-5.01
S2	12.0	33.5	151.36
N2	12.7	39.5	80.85
K1	23.9	25.7	124.35
O1	26.9	17.4	53.64

Table 4.2 Tide components data used in this research

4.6 Model calculation conditions

Longitude $69^{\circ}82'$ - $70^{\circ}46'$ E and Latitude $22^{\circ}26'$ - $23^{\circ}00'$ N bound the study area, the Gulf of Kachchh. The model domain, the Gulf of Kachchh is divided into 37 equal grids in north-south direction and 78 grids in west-east direction. Although fine resolution was desirable to account for the complicated Gulf bottom topography, a coarse grid system of 2 km was adopted in the horizontal direction, based on availability of bathymetry data and to save computational time. In the vertical direction, the Gulf water column was divided into 5 computational levels with a thickness of 5 meters for the first 4 top levels. The fifth level was considered from 20 m up to the bottom.

The bathymetry map (as shown in Figure 4.2) was grided in the same way as that of model domain. The bottom topography file was prepared using

average bathymetry values within each grid and this bottom topography file was used in the present model.

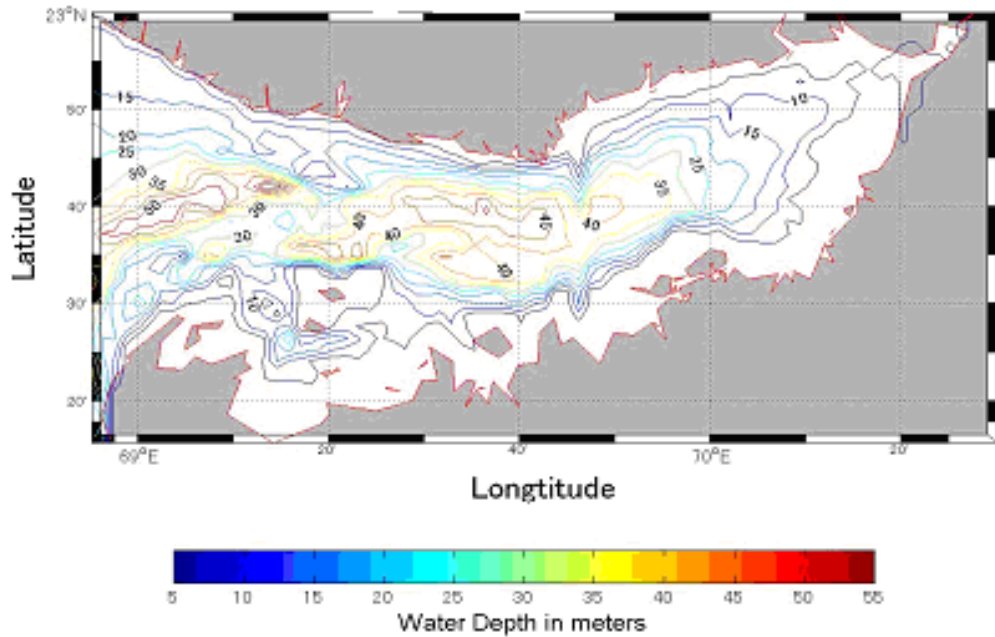


Figure. 4.2 Detailed depth contour map of the Gulf of Kachchh.

In COSMOS model, monthly mean river run-off, of all rivers, which are draining in Gulf of Kachchh, are needed along with temperature and salinity values at the mouth of river. Though input from seasonal, small rivers draining in Gulf is marginal, 3 river's run-off input is considered in this study. The run-off from rivulet Machhu, Demi and Phul are considered and their run-off are listed in Table 4.3

River	Run-off in m ³ /s
Adhoi	2.1
Sakara	4.0
Jhinhjoda	1.0
Phuldi	24.0
Machhu	476.0
Demi	438.0

Table 4.3 River runoff to the Gulf of Kachchh

In this modeling study, wind data retrieved from QuikSat satellite is used due to non-availability of in-situ measurements. Ocean surface winds over Gulf oceans are derived from the observations made by the scatterometer SeaWinds on QuikSCAT mission.

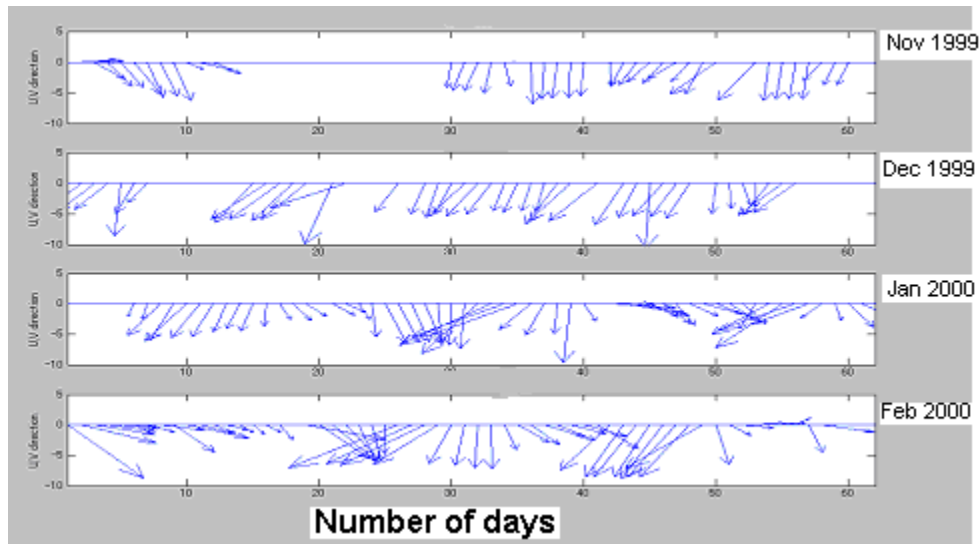


Figure 4.3 Wind speed variations over the Gulf of Kachchh estimated from Quikscat data from Nov. 1999 to Feb. 2000

Figure 4.3 shows the mean wind velocity over Gulf of Kachchh from Nov. 1999 to Jan. 2000. It seems that in the winter season, wind velocity over the Gulf is less than 10 m/s and wind direction are generally from north. Table 4.4 lists the mean wind speed over the Gulf in winter season. The mean value used in the model is 4.1m/s is from the north as is usually in the whole month of Nov. 1999, which can also be seen in Figure. 4.3.

	U m/s	V m/s	Speed m/s
Nov. 1999	-0.02	-4.14	4.1
Dec. 1999	-1.93	-5.45	5.8
Jan. 2000	-0.10	-4.20	4.2
Feb. 2000	0.79	-3.94	4.0

Table 4.4 Mean wind velocities over the Gulf of Kachchh from QuickSCAT data

The other meteorological condition include parameters like wind velocity over the Gulf, solar irradiance, day-length, cloud fraction, air temperature and relative humidity. Air temperature, relative humidity and cloud fraction are obtained from Da Silva et al. (1994) climatic data sets from 1984 -1991.

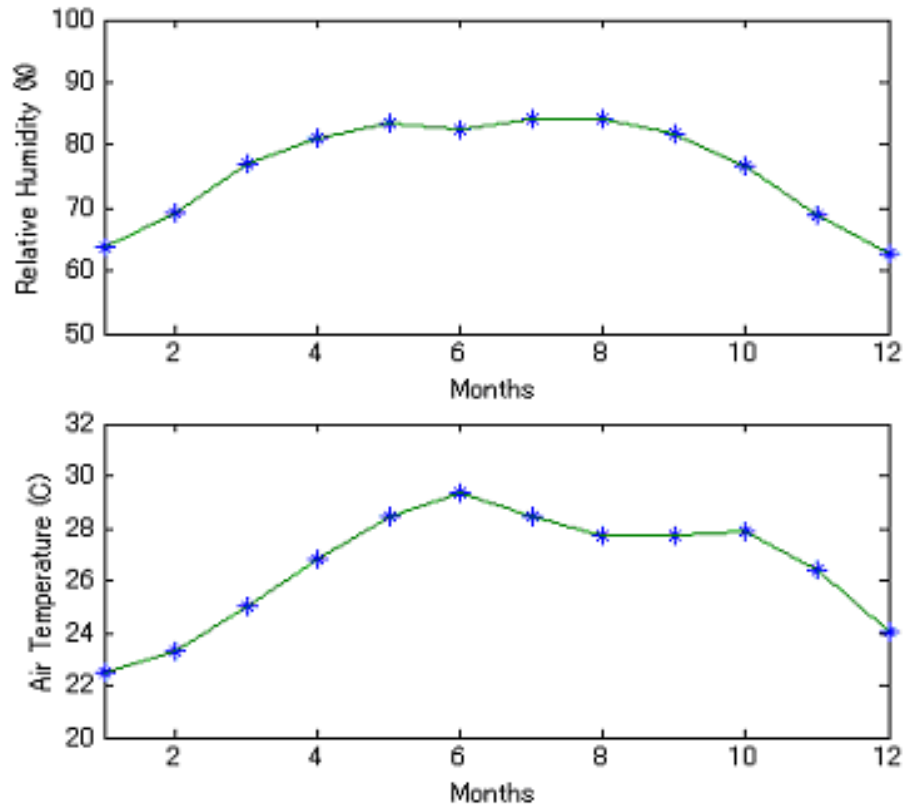


Figure 4.4 Relative humidity and air temperature variation around Gulf of Kachchh

Figure 4.4 shows the air temperature and the relative humidity above sea surface. It can be noticed that the temperature changes from 22^o to 29^o C whereas; relative humidity varies between 60 and 80%. The coefficients of eddy viscosity and diffusivity are taken to be equal to 850 m²/s (Unnikrishnan et al. 1999). Surface solar irradiance in the Gulf of Kachchh is calculated using software (Platt et al., 2000). For simulation of the model, time step of 30 seconds is used. The heat flux was evaluated as the sum of short-wave incoming solar radioactive, long-wave back radioactive, sensible and latent heat fluxes. In the present model, wind stress, air temperature, relative humidity, cloud fraction,

irradiance etc. were all assumed to be spatially uniform and averaged over the model domain.

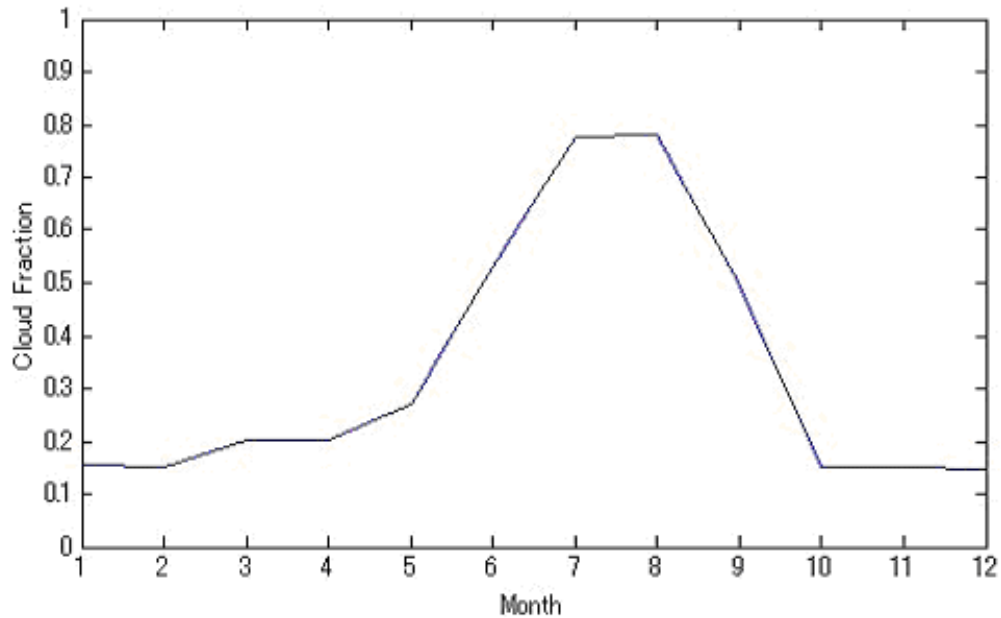


Figure 4.5 Cloud fraction over the Gulf of Kachchh in one year (after Da Silva et al. 1994)

Figure 4.5 shows the cloud fraction in this area and has less than 20% cloud coverage from Oct. to May next year. It also shows that Gulf of Kachchh has two different seasons, i.e., wet season from May to Sept. and dry seasons for other months.

4.7 Assumptions and conditions

After considering the availability of the wind data, NOAA/AVHRR data and the limited field data, the model was simulated for the November and December months of 1999. The initial conditions and the meteorological data chosen for the model are as shown in Table 4.5.

Table 4.5 Simulation conditions used in Gulf of Kachchh model

Items		Contents
1. Grids		77x38 grids with grid resolution: 2km
2. Layers		First layer 0 - 5 m 2 nd layer 5 - 10 m 3 rd layer 10 - 15 m 4 th layer 15 - 20 m 5 th layer 20 - bottom
3. Open boundary	Tide conditions	M ₂ , S ₂ , N ₂ , K ₁ , O ₁ components are considered, the parameters are shown in table 2.
	Temperature and salinity profile	The in-situ data measured in 1997 is used shown in Fig 2.1
4. Other Parameters	Coriolis coefficient	5.62E-5 s ⁻¹
	Bottom friction coefficient	0.0026
	Surface friction coefficient	0.0013
	Coefficient of eddy viscosity (horizontal)	8.5E+5 cm ² s ⁻¹
	Coefficient of eddy diffusion (horizontal)	8.5E+5 cm ² s ⁻¹
5. River Discharge		Phuldi, Machhu and Demi rivers run-off were used as shown in Table 3
6. Meteorological conditions	Wind velocity	Wind velocity data retrieved from QuikSat sensor are used and shown in Fig. 2.3 and Table 4
	Solar irradiance	711 cal/cm ²
	Solar zenith	0.84
	Air temperature	26.4
	Relative humidity	68.7%
	Cloud fraction	0.11
7. Time step	30 seconds	30 days from Nov.1 – 30, 1999

Table 4.6 Output parameters retrieved after running the model.

	Output Parameters of model	Units
T	elevation of water surface	theta (cm)
u	x-directional flow velocity	u (cm/sec
v	y-directional flow velocity	v (cm/sec)
w	vertical flow velocity	w (cm/sec)
r	water density evaluated from eqs. Of state	row (g/cm ³)
t	water temperature : temp	(deg.c)
c	concentration of chlorinity	cl (0/00)
p	mean pressure in each vertical level	p (g/cm/sec ²)
	density of turbulent energy	e (ergs/unit mass)

Time factor : Start time : 86,400 Sec --- 1day
Interval : 86,400 Sec --- Par day
End time : 2,592,000 Sec -- 30 days

Table 4.7 Simulation control parameters

iteration start time	itstat:sec	0
iteration end time	itend:sec	2592000
iteration time step	dt :sec	6.00e+01
period of surface tide	intevl:sec	43200
computational mode of water temperature	ismflt	1
computational mode of chlorinity conc.	ismflc	1
computational mode of turbulent energy	intflg	3
computation start time of nonlinear	inlnst:sec	0
computational step of nonlinear terms	nlnstp	1
computational step of horizontal eddy viscosity terms	nvsstp	1
computation start time for water temp. Distribution	itmstp:sec	10
computational step of temperature	ntpstp	3
computation start time of chlorinity	iclnt:sec	0
computational step of chlorinity	nclstp	3
computation start time of sgs energy (turbulent energy)	iestat:sec	0
computation step of sgs energy	nestep	1
seashore current computation	irdfg	0
initial condition input mode	iniset	0
initial value file input start time	initst:sec	0
boundary value file input start time	ibndfl:sec	0
flag for boundary connection into the subregion	ibdfg	0
output start time into boundary connection file	ibndst:sec	0
output end time into b.d connection file	ibnded:sec	0
residual current computational mode	iresid	1
file input start time for residual current computation	irestm:sec	86400
end time, same as above	iresed:sec	2592000

Table 4.8 Constants used in model.

Constants used in model	Units	Values
acceleration of gravity	(g)	9.80e+02 (cm/sec**2)
coriolis parameter	(f0)	5.62e-05 (rad/sec)
density of air	(rowa)	1.30e-03 (g/cm**3)
drag coefficient	(gama2)	1.30e-03
specific heat of the seawater	(cv)	1.00e+00 (cal/(g*deg.c))
zero check parameter	(eps1)	1.00e-06
instability check parameter	(eps2)	1.00e-03
mollecular viscosity in the	intflg=2,3:rnw0	5.00e-02

vertical direction		
vertical momentum exchange coeff. In neutral stable state	(intflg=2:rnw1)	5.00e-02
mamayev constant	intflg=2,3:rzn	1.00e+01
molecular diffusivity in the vertical direction	intflg=2,3:rnk0	5.00e-02
vertical mass exchange coeff. In the neutral stable state	intflg=2:rnk1	5.00e-02
mamayev constant	intflg=2,3:rzk	3.33e+00
constant in the turbulent viscosity proportional const	intflg=3 : cmieu	9.00e-02
turbulent prandtl number	intflg=3 : prt	1.00e+00
prandtl-shumidt number	intflg=3:sk	1.00e+00
constant in the dissipation term	intflg=3 : cd	4.00e-01
von-karman constant	intflg=3:k	4.00e-01
upwind parameter for horizontal inertia term in momentum equations	(xihv)	1.00e+00
same way, for the vertical term	(xivv)	2.00e-01

Chapter 5 – MODEL RESULTS AND VALIDATION

Chapter 5

MODEL RESULTS AND VALIDATION

5.1 Introduction

Considering the model simulation requirement and availability of data, two separate initial input cards for two months November–99 and December–99 were prepared. Several Fortran –77 programs constitute the COSMOS hydrodynamic model. These programs are executed along with initial input card to simulate the hydrodynamic model. Using an Alpher mini-computer system at the Center for Environmental Remote Sensing (CEReS), Chiba University, a hydrodynamic model was simulated separately twice for two different months, November and December of 1999. In this chapter model validation and results of model are presented and discussed.

Model validation problem arise as all simulation models contain both simplification and abstractions of the real world system, and as such no model is absolutely correct in the sense of a one-to-one correspondence between itself and the real world. By neglecting the strict definitional sense of the word “valid”, a valid model can be develop by making certain that there is very close correspondence between the model and the coastal dynamical system. This is done by building a model that has high face validity. The model is valid if it accurately predicts the performance of the coastal system. If this is not achieved then it is necessary to examine and change the structure and assumptions of the model. With repeated adjustments to these, a valid model can be developed. The COSMOS model being simplification and abstraction of the real coastal ecosystem, validation is attempted by running simulation for two different months and then testing it’s performance against known in-situ and satellite results.

The numerical model was simulated for the period starting from Nov. 1, 1999 for 30 days of the month. And then once again model is simulated for the period starting from 1 December till 31st of the same month. At the initial stage, the flow field was assumed to be stationary. The simulated results of the first day were not used as the model was allowed to settle for one day. Initially, several runs of the model have been carried out to test efficiency in reproducing tides and currents in computational domain. The model has been validated by comparing the simulating parameters like temperature, salinity, tides, currents etc. at the diagnostic (monitoring) points with the measured data available for those locations.

5.2 Modeling tidal velocity currents during ebb and flood tide

The tidal current values for two days 12th and 13th of Dec for time 0400 hrs and 2100 hrs respectively were extracted and plotted. Figure 5.1 shows majority tidal currents of high intensity (2.5 m) at the open border near Okha and is moving from the mouth towards the head of the Gulf representing high tide condition. And in tide table also same time of the same day is marked as high tide. Similarly, figure 5.2 shows tidal currents of low intensity traveling from the head towards the mouth of the Gulf, representing ebb currents and low tide situation that is also indicated in the tide table.

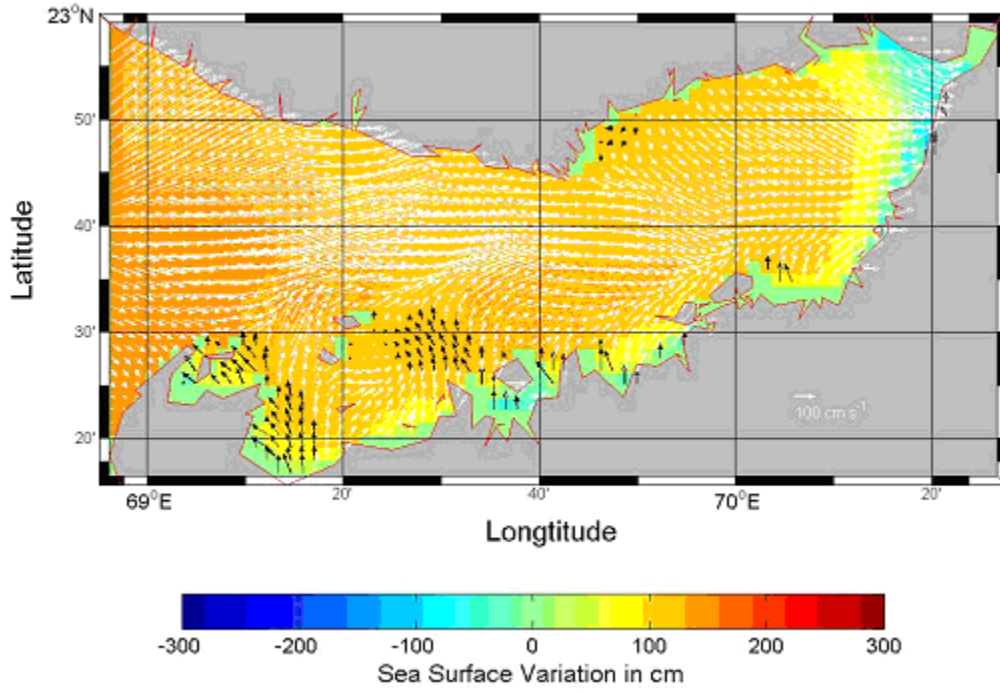


Figure 5.1 Model result showing high tide condition on 13th Dec 1999 at 0400 hrs.

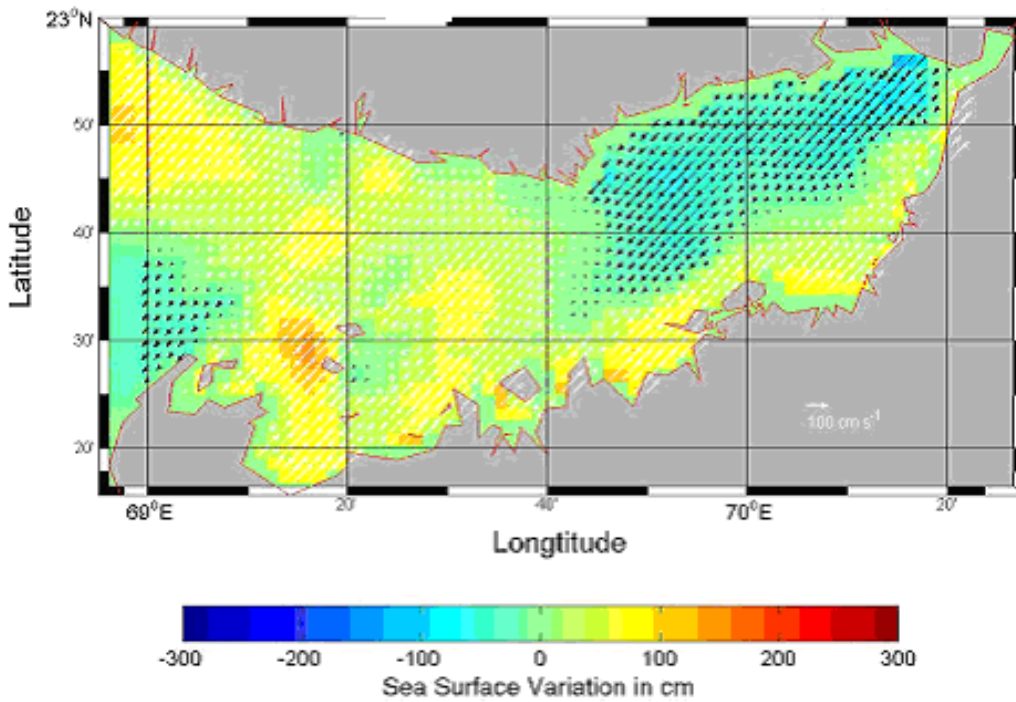


Figure 5.2 Model results showing low tide condition on 12th Dec 99 at 2100 hrs.

5.3 Modeling surface current velocity distribution

Figure 5.3 shows the model result of ocean surface current velocity overlaid on the sea surface variation. Figure 5.3 is showing surface current distribution at 06:00, Nov. 15, 1999, half an hour after high tide. Surface variation changes from -68 cm to 39 cm and current travels from the head to the mouth of the Gulf with the maximum speed of 200 cm/s. Three hours later, the distribution of current and sea surface variation is shown in Figure 5.4. The sea surface variation in the Gulf is from -173 cm to 54 cm with the maximum current speed of 209 cm/s. High tide currents are moving from the mouth towards the head of the Gulf and tide current direction is reverse as compared with Figure 5.3. Variation in the current velocity due to the presence of the islands is clearly seen in these figures. As far as the tide magnitude is concerned, the model simulation shows that the maximum current velocity is accelerated up to 200 cm/s.

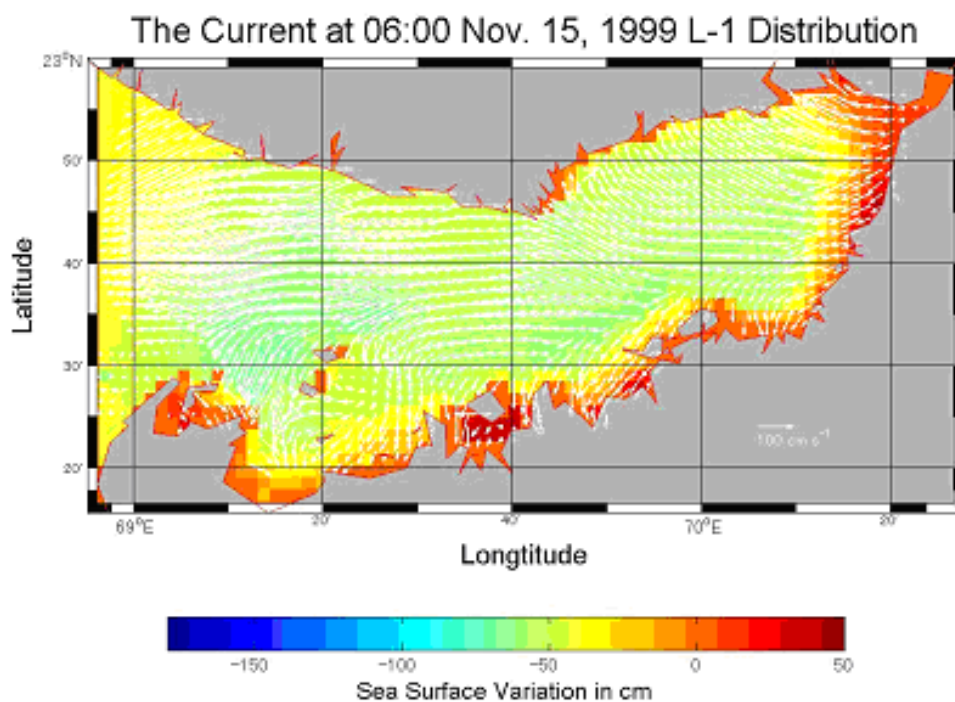


Figure 5.3 Surface current velocity distributions from 3-D numerical model (after high tide at Okha around open boundary)

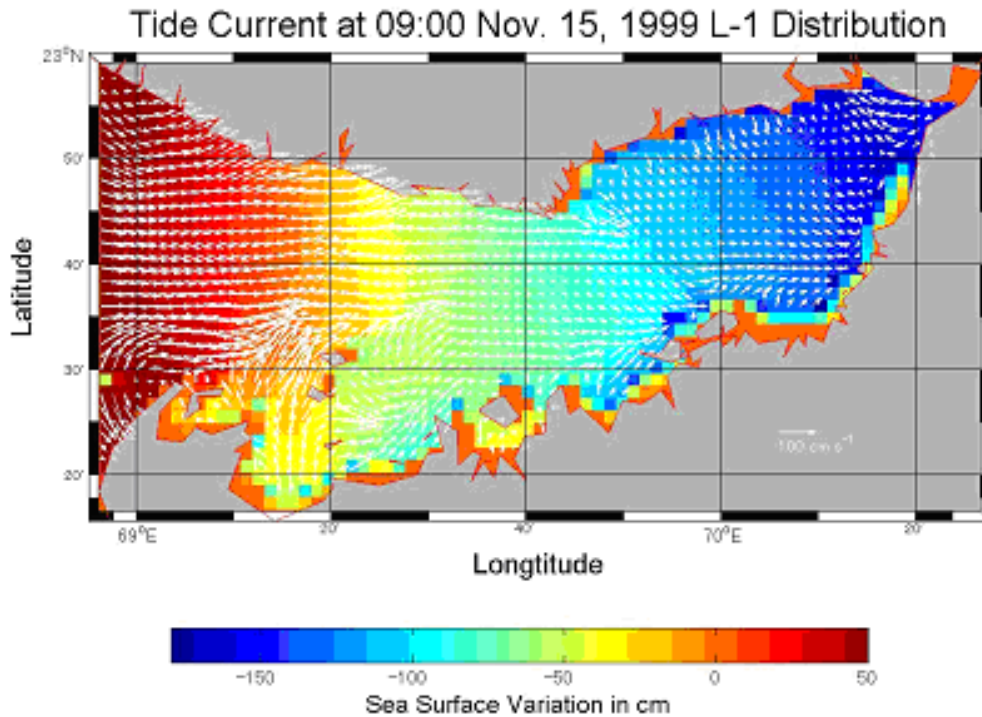


Figure 5.4 Surface current velocity distribution from 3-D numerical model (before high tide at Okha)

The current velocity distribution at 09:00 on Nov. 15, 1999, shown in Figure 5.4, have almost similar pattern as compared with Sinha et al. (2000) results (Figure 5.5). The major currents are traveling from the mouth to the head of the Gulf, especially very strong current with more than 2.5m/s shown at the open boundary and the northern part of Bhoidar, Naro Islands. The result of this study shows a rather large value in the inner region in the Gulf of Kachchh.

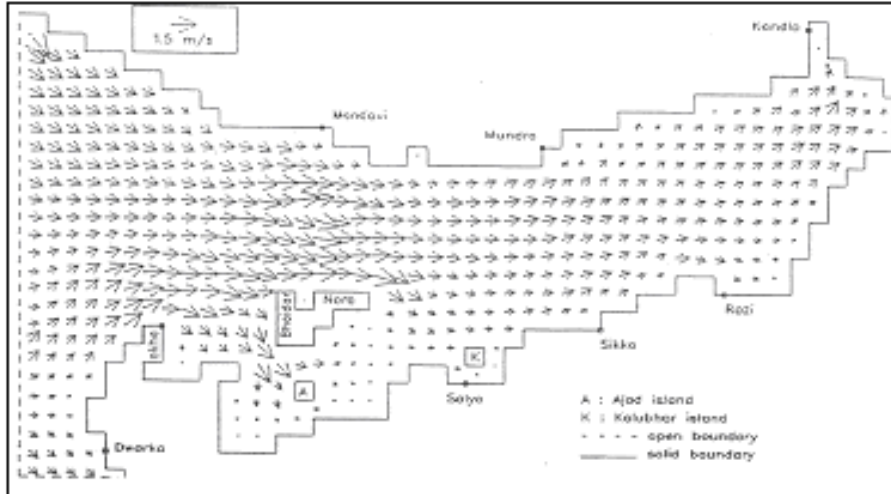


Figure 5.5 Tide stream current one and half hour before high at Okha

Prandle et al. (1984) used 2D model to investigate tide currents in the Gulf of Kachchh without considering influence of other factors except M_2 tide components. It seems that surface current velocity in the Gulf is mainly controlled by the tide system. The COSMOS numerical modeling results also confirmed this conclusion after setting wind speed zero in the initial conditions of model.

5.4 Modeling residual current distribution and validations

Residual current distribution in the Gulf of Kachchh at the surface for Nov-99 is shown in Figure 5.6. Residual currents travel from the mouth at the open boundary area with higher velocity of around 15cm/s towards the head of the Gulf. Two maxima residual current regions can be found in the east and west of the Island Mandro with a speed more than 25 cm/s. However, majority of the residual currents, in the middle layer, have magnitudes of less than about 5 cm/s as shown in Figure 5.7.

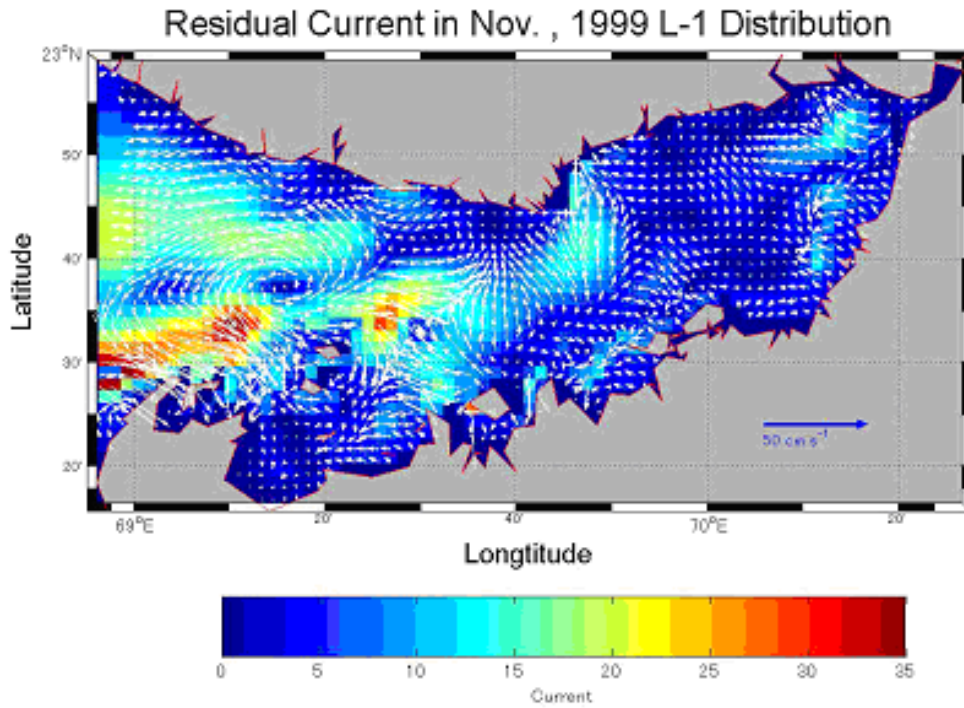


Figure 5.6 Residual current velocity distribution at the surface of the Gulf of Kachchh

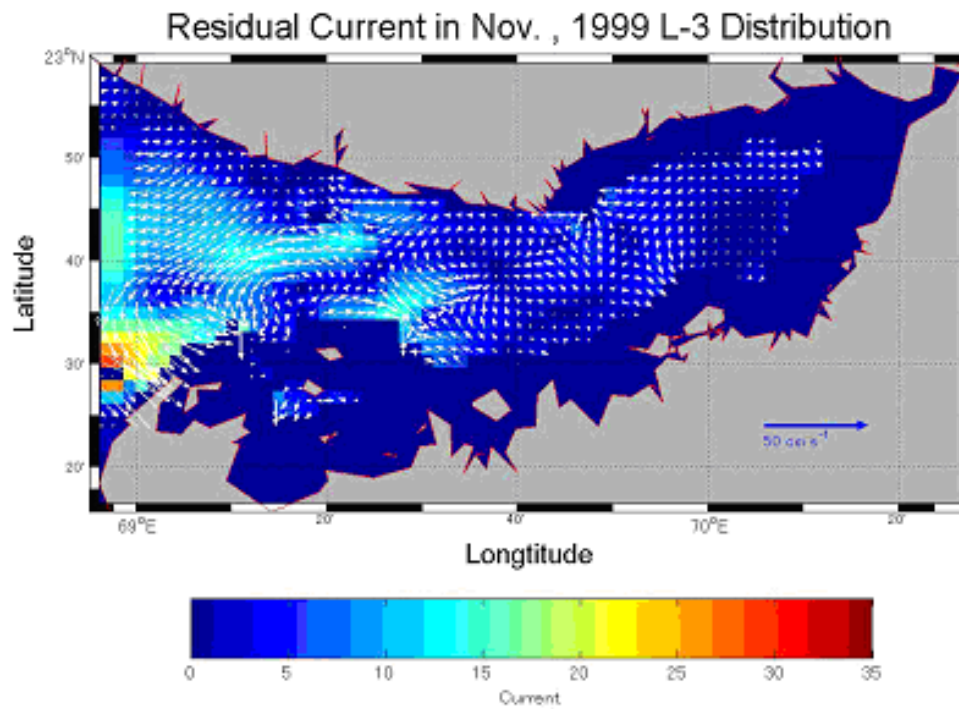


Figure 5.7 Residual current velocity distribution of the Gulf of Kachchh - the middle layer

An anticyclone eddy of residual current can be clearly seen around this area, which was also reported by Prandle et al. (1984), Unnikrishnan et al. (2000) and Sinha et al. (1999). It is interesting to note that several convergence and divergence regions are visible in the middle of Gulf. In the subsurface layer and bottom layer of the Gulf of Kachchh, the main features of the residual current field show little difference among different layers but the current speed decreases from the surface layer to bottom. Moreover, in the deep area of the Gulf, water motion is gradually ceasing.

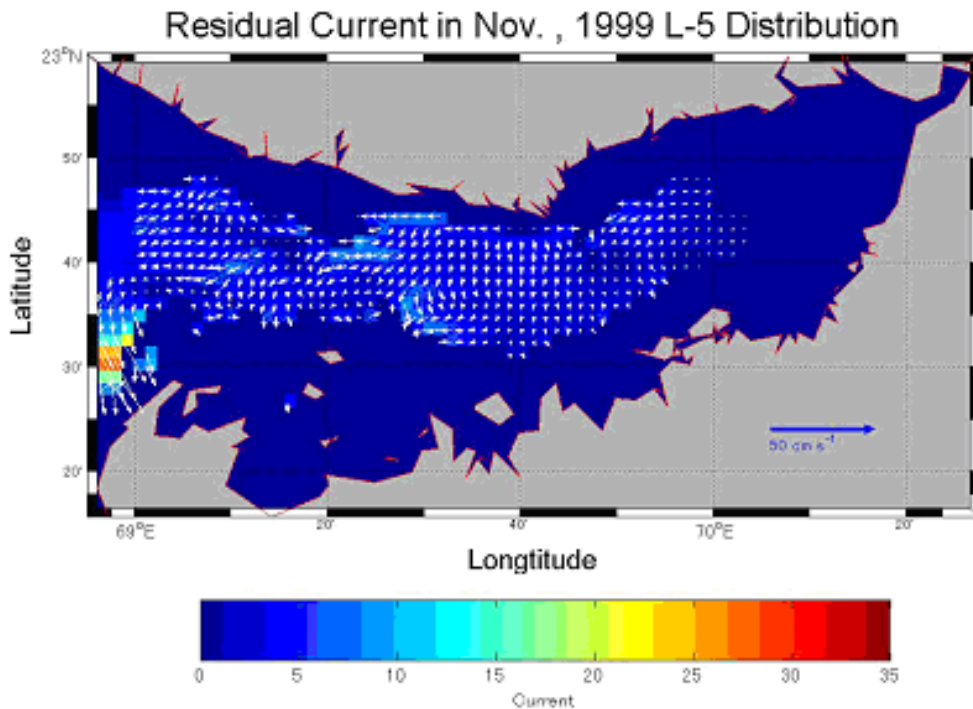


Figure 5.8 Residual current velocity distribution of the Gulf of Kachchh in the bottom layer.

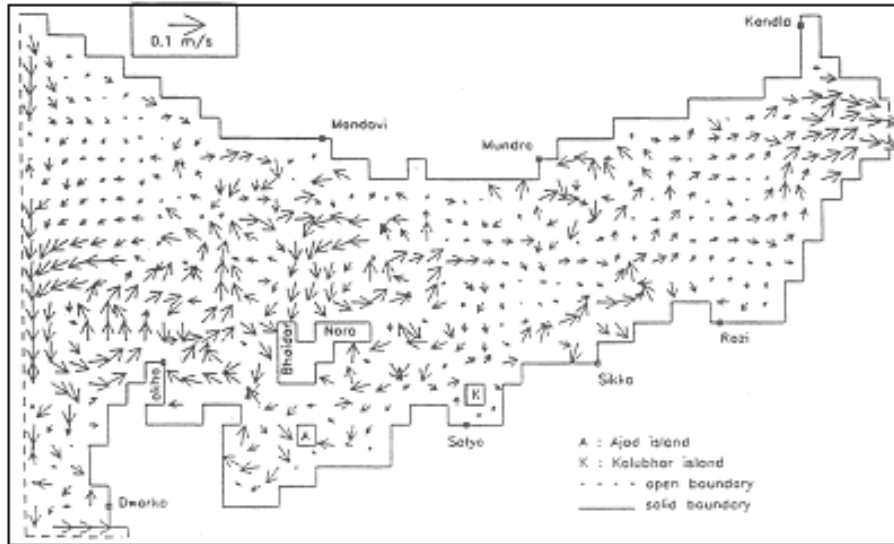


Figure 5.9 Tide residual current distribution in the Gulf of Kachchh at the surface (Sinha et al. 2000)

Figure 5.7 and Figure 5.8 show the residual current distribution in the middle and bottom layer. The main features are almost same like the surface layer but with smaller value, indicating barotropic approximation is reasonable in Gulf of Kachchh. Figure 5.9 shows 2D model results obtained by Sinha et al. (2000). It can be seen that the main features are similar to COSMOS model results, however, some features are not very clearly represented which are influenced by vertical structure.

Residual current distribution in the Gulf of Kachchh for Dec-99, as shown in Figure 5.10, at surface level shows similar pattern as that of Nov-99 month. However, features like cyclonic eddy, convergence and divergence areas are seen more clearly. High current velocity towards the head is different. Residual currents distribution (without magnitude) for Dec-99 shows current pattern more clearly as seen in Figure 5.11.

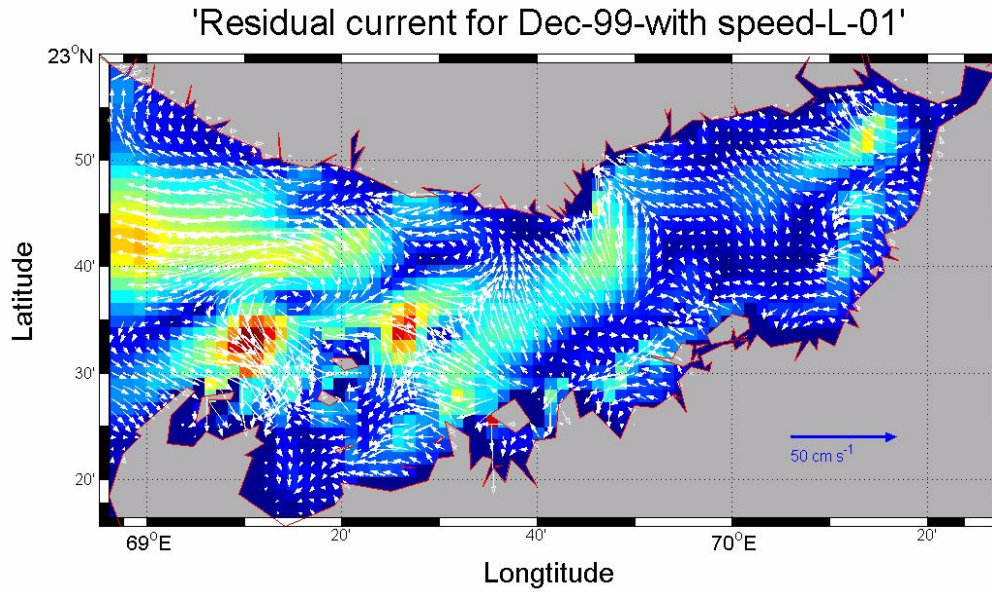


Figure 5.10 Residual current velocity distribution of the Gulf of Kachchh for December at the surface layer.

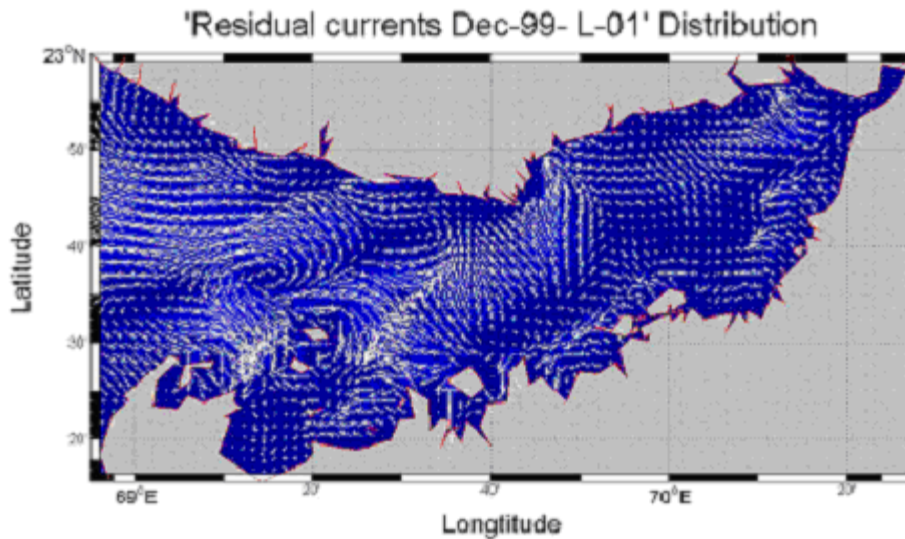
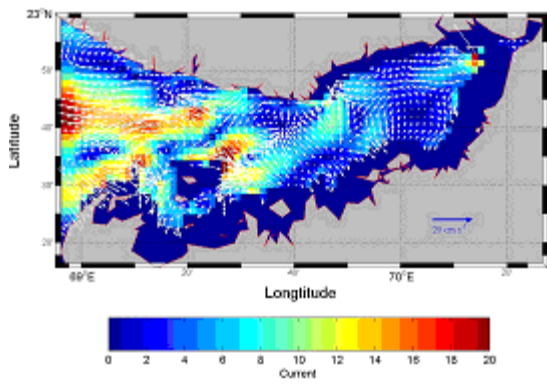
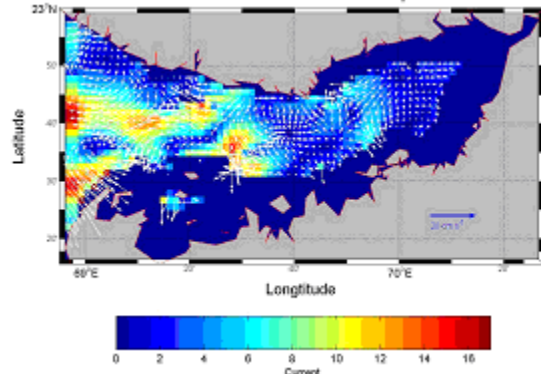


Figure 5.11 Residual current distribution of the Gulf of Kachchh for Dec-99

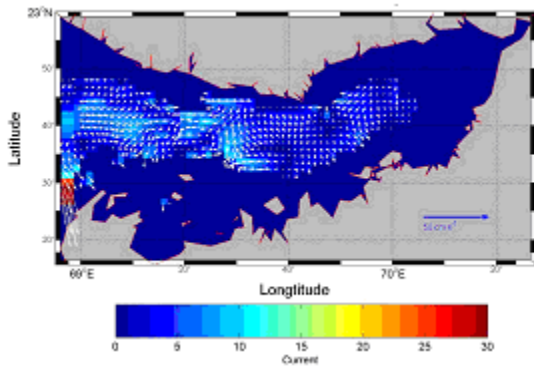
The residual currents at different layers are shown in Figures 5.12 respectively. It is noted that areas covered by higher magnitude currents remained the same, however, intensity of residual currents reduces as depth increases.



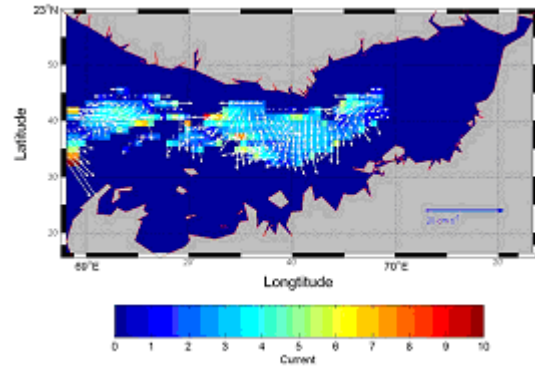
Layer 2



Layer 3



Layer 4



Layer 5

Figure 5.12. Residual currents with speed at different layers from surface to bottom.

5.5 Modeling of residual current velocity for constant depth

The simulation by 3D model was conducted during Dec-99, assuming fixed or constant depth at 30 meters. The residual current velocity pattern obtained is shown in Figure 5.13. If residual current pattern developed at the surface level with natural bathymetry is compared with pattern that form with 30 m fixed depth, it is noted that magnitude of the current reduces from 50 cm to 20 cm, however areas of high magnitudes almost remain the same. In case of fixed depth, areas of high magnitude spreads more as compared to other and the eddy pattern diminishes in flat bottom or fix depth condition.

Whereas in the simulation conducted for Nov-99, it was observed that areas with larger value of residual current are located in the area where depth changes rapidly. From these two evidences, it can be said that in the Gulf of Kachchh, change in topography is the most important factor in determining the distribution of residual current velocity. Unnikrishnan et al. (1999) also used model simulation to validate that the effect of topography on existence of the eddy, and found that the eddy disappears if constant depth condition is assumed in the model.

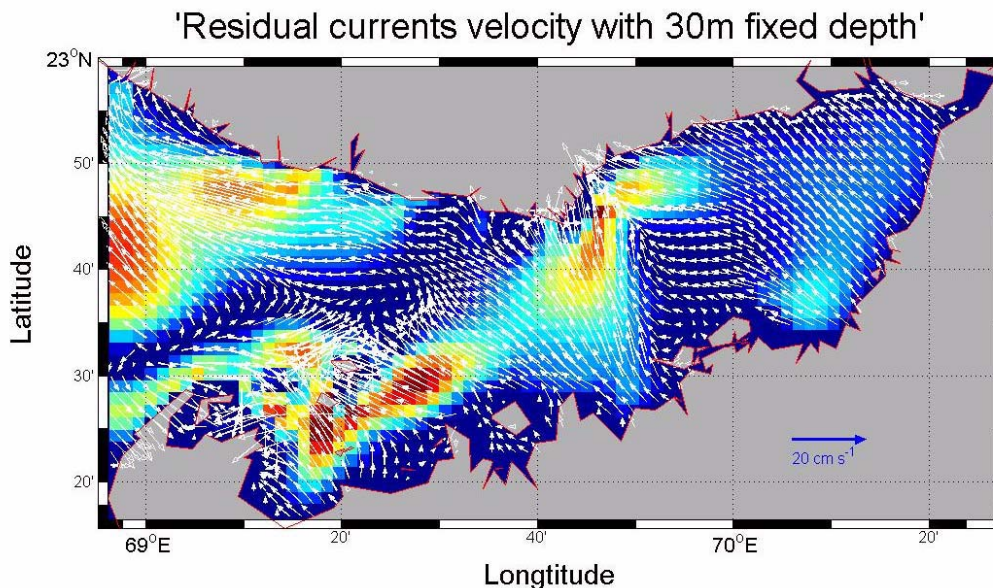


Figure 5.13 Residual current velocity distribution of the Gulf of Kachchh for Dec-99 assuming uniform depth of 30 m.

5.6 Tide features and tide mixing effects

The main characteristic of the Gulf of Kachchh is its high tidal variation. Shetye (1999) proposed that amplification of tide is due to a combination of quarter-wavelength resonance and geometric effect. To verify these model results and the amplitude and phase distributions of tide M_2 and K_1 components were obtained for Nov-99. Figure 5.14 shows that the amplification ratio for M_2 tide is about 2.3. The phase difference is about 90 degrees, and these results are comparable with Shetye (1999).

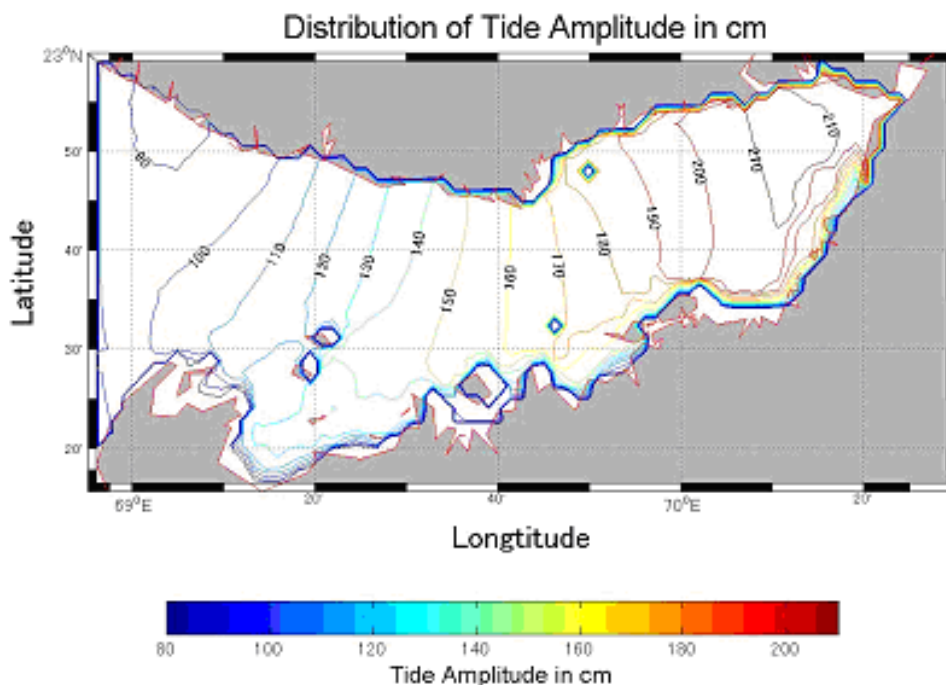


Figure 5.14 Tide amplitude of M_2 in Gulf of Kachchh

According to quarter-wavelength resonance condition, the tide period is equal to the resonance period if $T_r = 4L/(gH)^{1/2}$, then resonance period in the Gulf of Kachchh will be 16 hrs. After considering the bottom friction and other factors, Shetye (1999) proposed that the resonance period is around

11.5 hrs. It means that M_2 tide is almost with the resonance period and should have the maximum amplification.

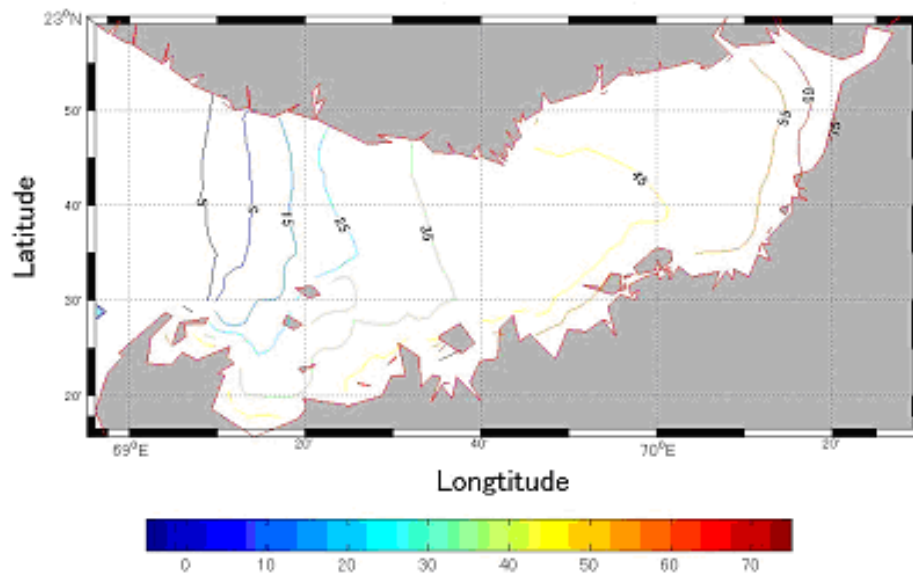


Figure 5.15 Phase distribution of M_2 Tide (in degrees) in the Gulf of Kachchh

For comparison, the second tide component K_1 tide in Gulf of Kachchh was also re-analyzed, and the results are presented in Figure 5.16 and Figure 5.17. The tidal amplitude variation change from 55 cm to 60 cm in the whole Gulf and phase difference is around 24 degree. It concludes that no resonance effect was observed in K_2 tide components.

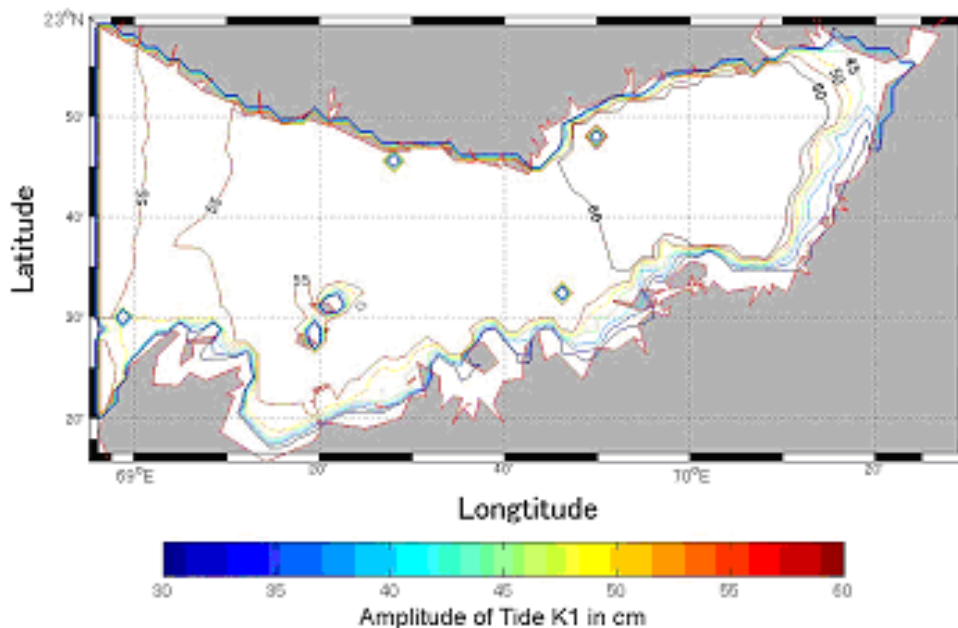


Figure 5.16 Tide amplitude distribution of K_1 in cm in the Gulf of Kachchh

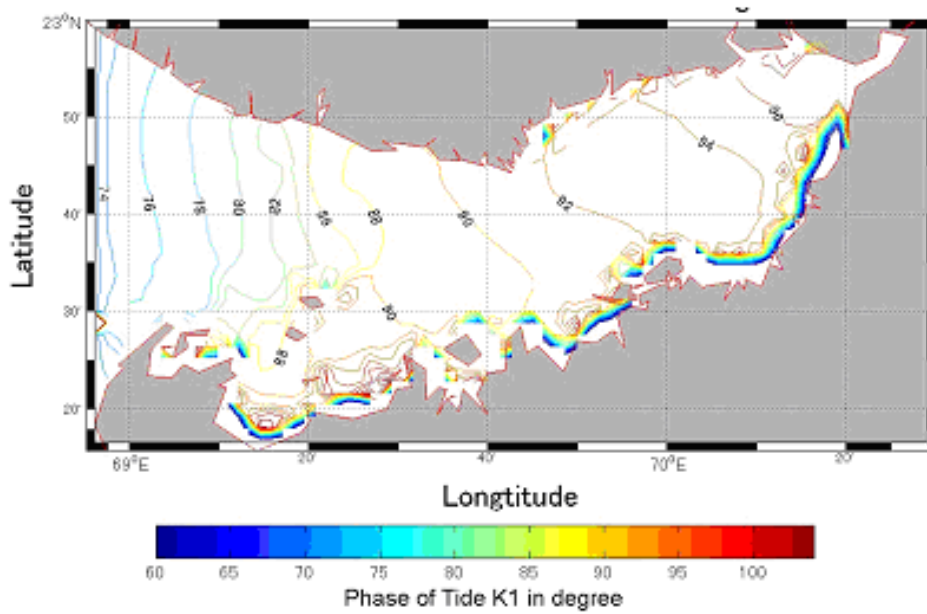


Figure 5.17 Distribution of phase of Tide K_1 in degree in Gulf of Kachchh

The amplification of tidal components M_2 and K_1 were again tested by modeling other data set for Dec-99 and the results obtained are presented as below:

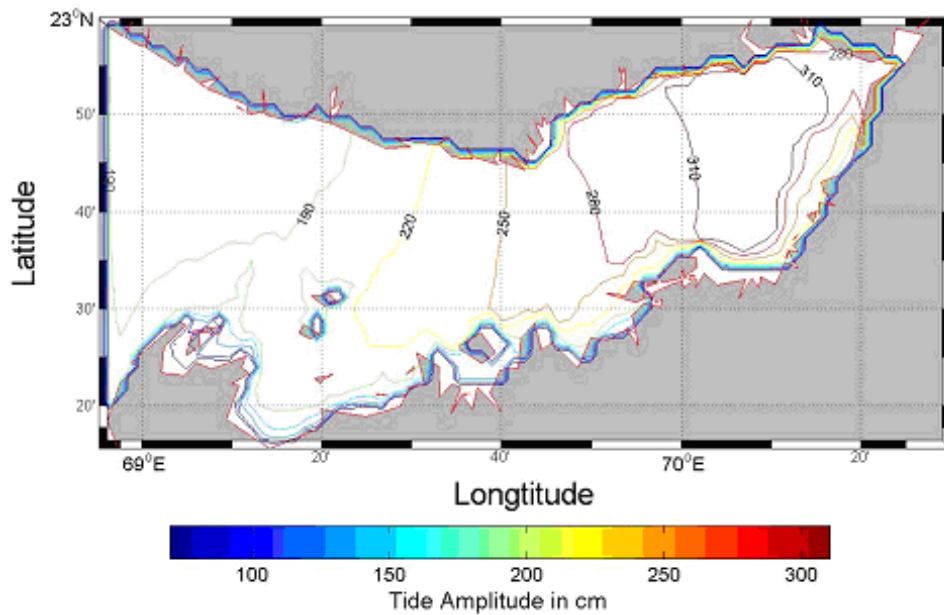


Figure 5.18 Distribution of Tide amplitude of M_2 in cms in Gulf of Kachchh

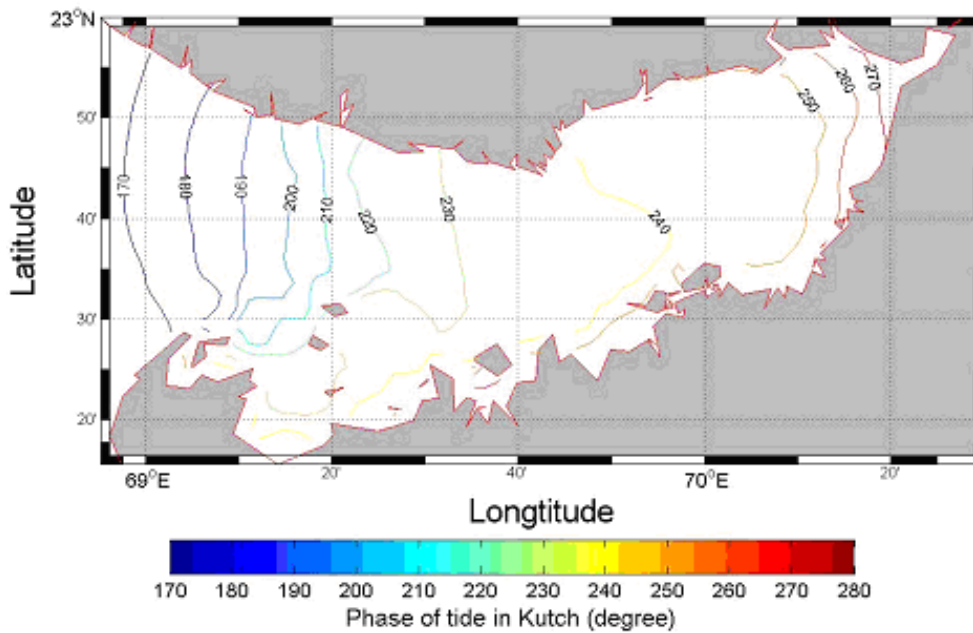


Figure 5.19 Distribution of Tide phase of M_2 in Gulf of Kachchh

The model results (Figure 5.18) for December months also showed that the amplification ratio for M_2 tide is about 2.3. Whereas, the phase difference (Figure 5.19) is around 100 degrees.

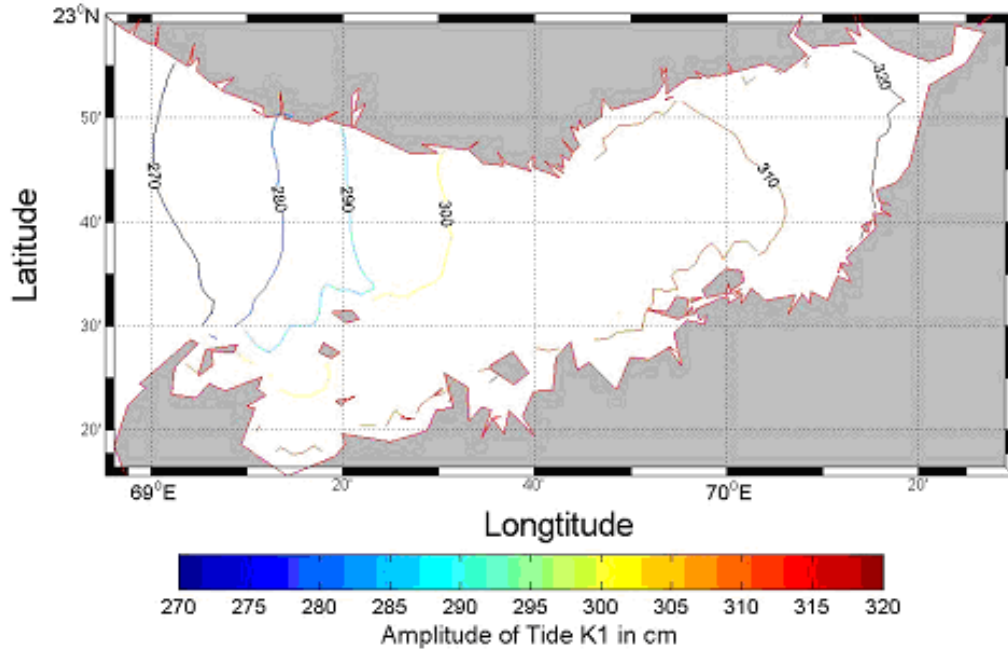


Figure 5.20 Distribution of Tidal amplitude of K_1 in cm in the Gulf of Kachchh

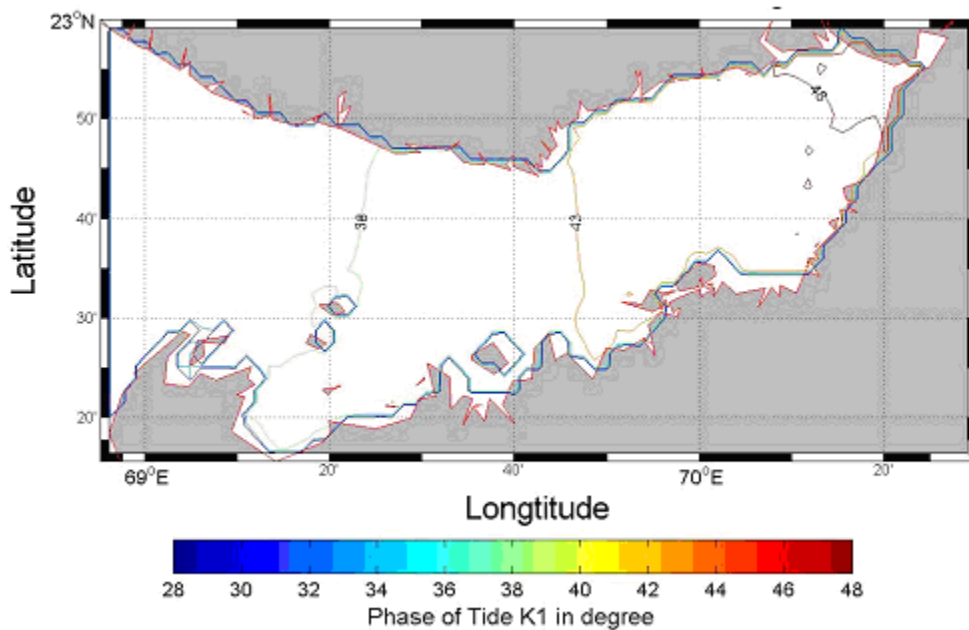


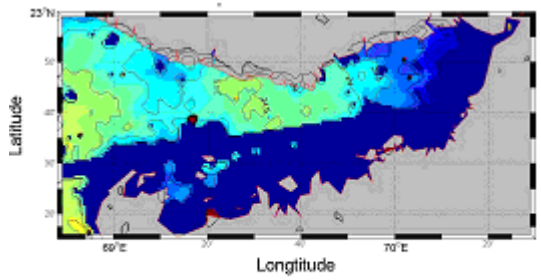
Figure 5.21 Distribution of Tide phase of K_1 in degrees in Gulf of Kachchh

The model results for Dec-99 (Figure 5.20) also shows that the amplitude variation for Tide K_1 is only 60 cm in the entire Gulf and phase

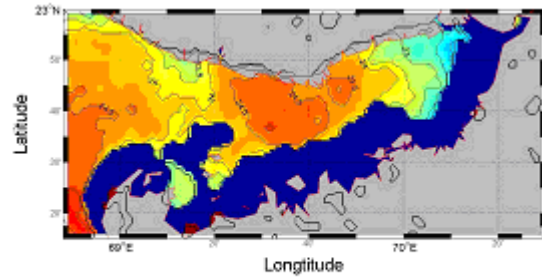
difference (Figure 5.21) is just 12-20 degrees. This supports the fact that no resonance effect is observed in K_2 tide component.

5.7 Sea surface temperature and salinity distribution

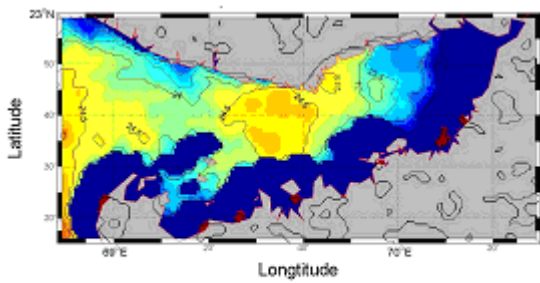
Sea surface temperature derived from NOAA/AVHRR was used to validate the model results. The sea surface temperature for four different days in the month of December (Figure 5.22) and six days of November (Figure 5.26) was derived from NOAA/AVHRR. It is observed that the temperature decreases from the mouth towards the head of the Gulf. For the same four days of December month (Figure 5.23,24) and six days of November (Figure 25) for the same time, temperature was derived after simulation. The model results show the similar trend of the temperature decreasing from the mouth to the head of the Gulf gradually. However, when the wind influence was not considered in the numerical model, the distribution of sea surface temperature in the Gulf was little different. This result suggests that wind speed is an important factor in adjusting SST variation. This demonstrates the importance of heat flux at the air-sea interface, especially in considering eco-dynamical system in the Gulf.



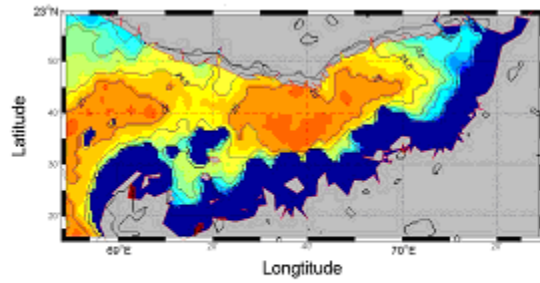
Date: 17-Dec-1999 Time:10:59 hrs



Date: 16-Dec-1999 Time: 11:10 hrs.

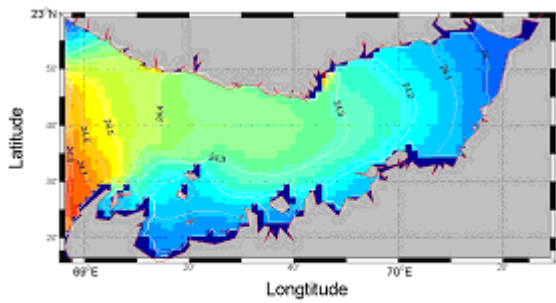


Date 15-Dec-1999 Time: 11:22 hrs

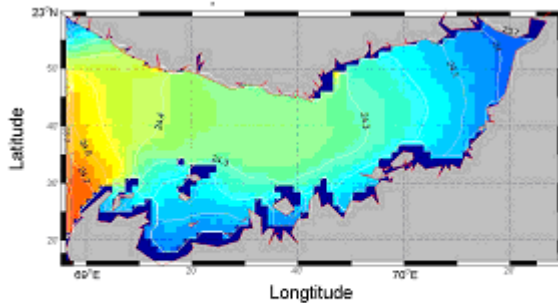


Date: 07-Dec-1999 Time: 11:01 hrs

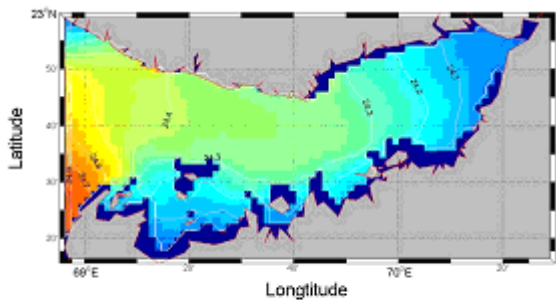
Figure 5.22 Sea surface temperature measured by NOAA/AVHRR for Dec-99



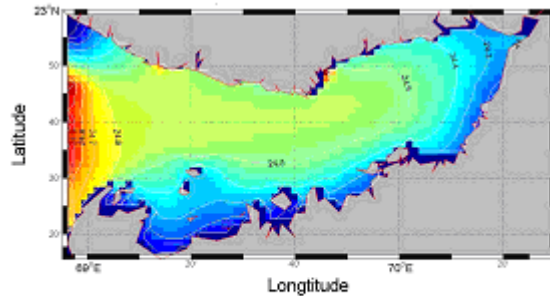
Date:17-Dec-99 Time: 11:01 hrs



Date:16-Dec-99 Time: 11:01 hrs



Date:15-Dec-99 Time: 11:01 hrs



Date:07-Dec-99 Time: 11:01 hrs

Figure 5.23 Sea surface temperature in the first layer of the Gulf of Kachchh derived using COSMOS model

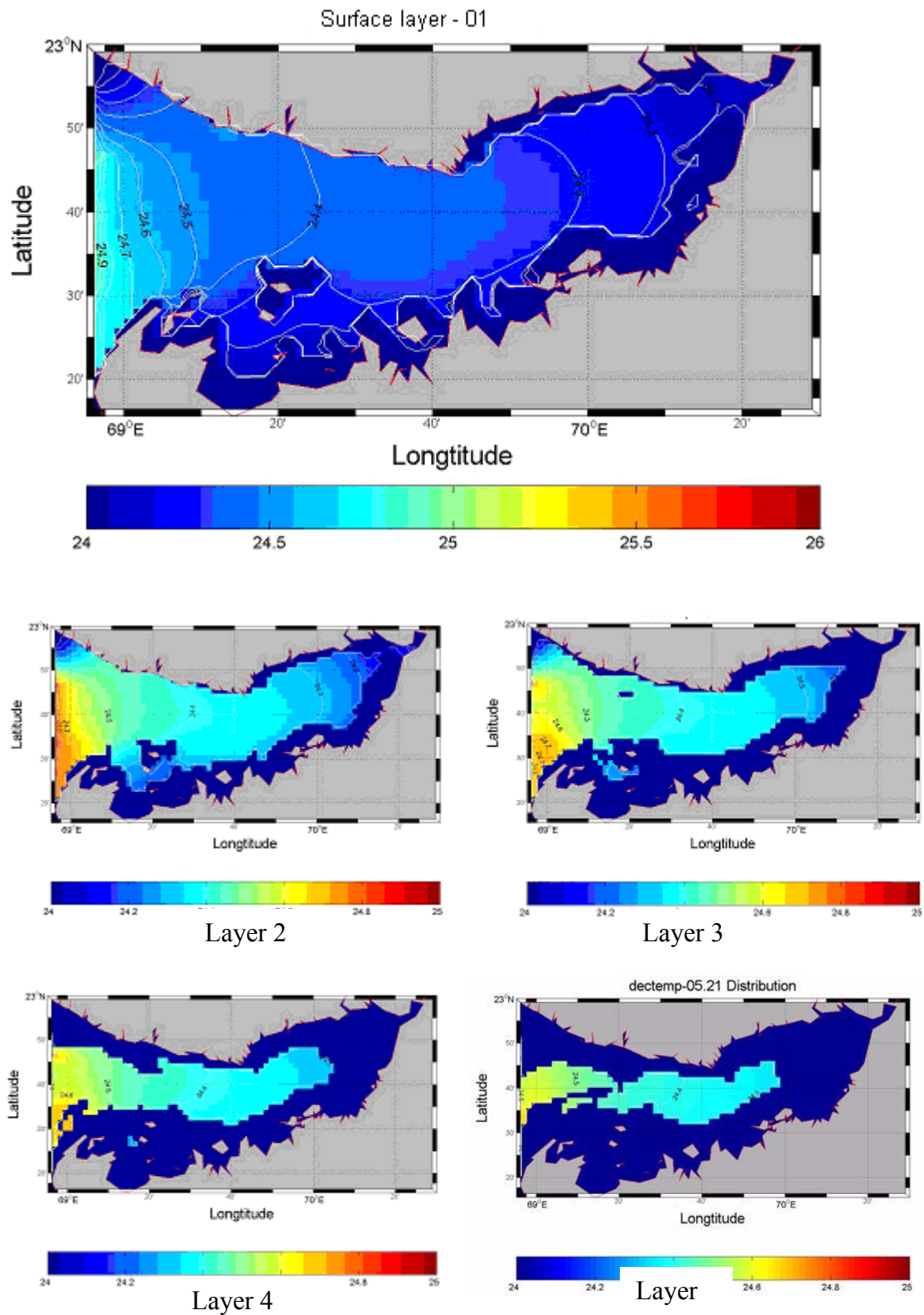


Figure 5.24 Sea surface temperature derived using COSMOS model for 5 different layers respectively for Dec-99.

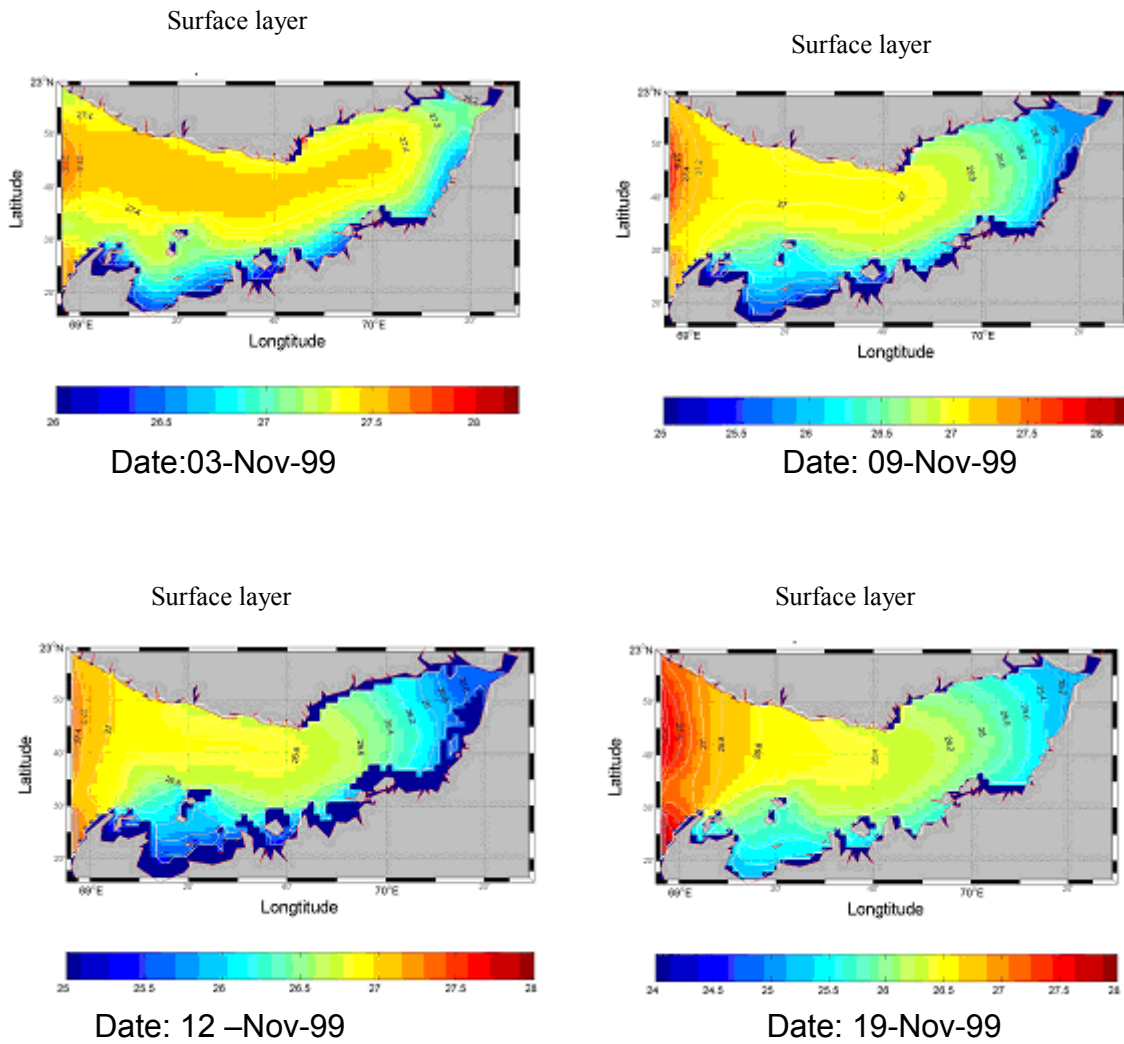


Figure 5.25 Sea surface temperature in the first layer of the Gulf of Kachchh derived using COSMOS model for Nov-99.

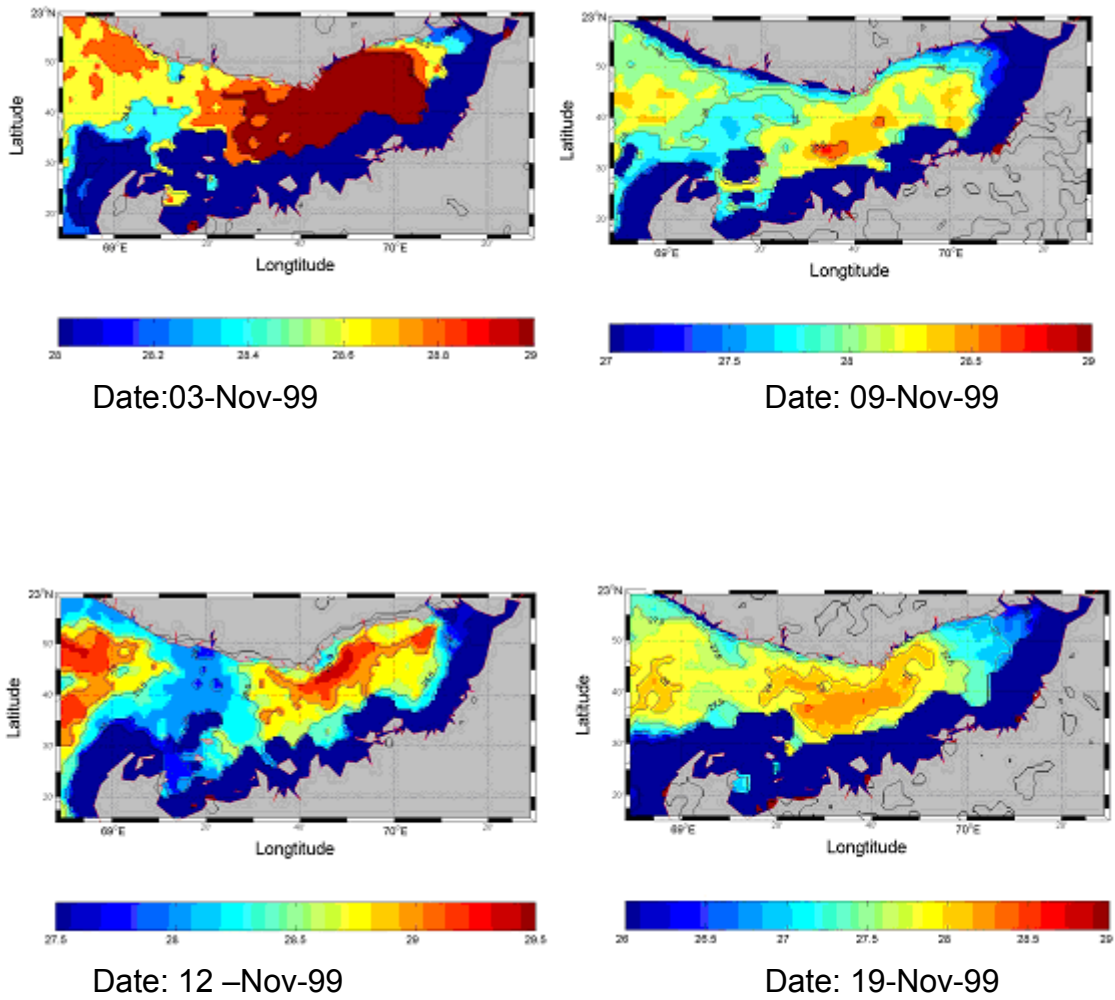


Figure 5.26 Sea surface temperature distribution measured by NOAA/AVHRR for Nov-99

Salinity distribution in the Gulf was also investigated using numerical model. The model results show high salinity concentration with the variation of about 36.09-36.13 psu. Almost no difference in salinity was noted with or without wind factor consideration. This result is also reasonable due to the fact that the precipitation and river run-off are the important factor in determining salinity distribution.

5.8 Summary

The COSMOS numerical hydrodynamic model was simulated using an Alpher mini-computer system for two months namely Nov-99 and Dec-99. After the simulation of the model, validation is necessary as models are simplifications and abstractions of the real world systems. Modeling of tidal velocity currents during ebb and flood tide was conducted and results were verified using a tide table. Surface current velocity distribution was obtained for Nov and Dec months and results were found in agreement with numerical results obtained by 2D model.

Residual current distribution for 5 depth-layers was obtained after the model simulation for Nov and Dec months. It was noted that areas covered by higher magnitude currents occupy the same position. However, intensity of residual current reduces as depth increases. Modeling of residual current velocity for constant depth showed depth variation certainly alters current distribution. Using model, tide features and tide mixing effect was studied and amplification of M_2 tide due to combination of quarter-wavelength resonance and geometric effect was verified. Sea surface temperature and salinity distribution was mapped and results were verified by comparing with NOVA/AVHRR satellite data.
